2014

A Low-Power Compact NQR Based Explosive Detection System

Xinwang Zhang
University of Nebraska-Lincoln, xzhang2@huskers.unl.edu

Nathan Schemm
University of Nebraska-Lincoln, nathan.schemm@huskers.unl.edu

Sina Balkır
University of Nebraska-Lincoln, sbalkir2@unl.edu

Michael W. Hoffman
University of Nebraska-Lincoln, mhoffman1@unl.edu

A Low-Power Compact NQR Based Explosive Detection System

Xinwang Zhang, Nathan Schemm, Sina Balkır, and Michael W. Hoffman

***Abstract*— Nuclear quadruple resonance (NQR) has been studied for explosive detection for years. Some prototype NQR-based detection systems have been reported, but were all designed from the laboratory perspective, with bulky sizes and high power consumption. To achieve a portable NQR-based detection system for field applications, a low-power compact system utilizing state-of-the-art semiconductor technologies is presented in this paper. Several novel circuits for the key modules are proposed, including a Class-D type power amplifier, a power multiplexing and matching network, a customized IC with integrated analog signal processing chain, and a microcontroller-based logic control unit. An advanced digital signal processor platform is employed for data collecting and processing. The customized IC is fabricated in 0.18 μm CMOS process. Test results on the prototype system show the effectiveness of the proposed solution and low power consumption as 2.12 W in the receiving state. The power efficiency of the proposed transmitting section is higher than 60%.**

***Index Terms*— NQR, explosive detection, Class-D power amplifier.**

I. Introduction

Nowadays, the society is confronting two severe safety issues which concern explosives. One is the global abandoned landmine problem. According to United Nations' estimate, approximately 80 million of landmines are still in place, mostly in the afterwar fields, of 85 countries around the world. There are 15000 to 20000 new non-military casualties every year, one third of which are children, caused by the numerous landmines [1]. On the other hand, terrorist bomb attacks, one of the most destructive terrorism actions, pose more cruel threat to civilians.

To help this situation, a wealth of effort has been dedicated by the researchers to find solutions for explosive detectors during the past several decades [2]. The most well-known and widely applied detection methods are metal detectors and ground penetrating radars because of their construction simplicity. Since their inherent mechanisms are to search for the containers of bombs and landmines, as expected, they suffer from a mass of false alarms caused by external detection circumstance changes. Inspired by the sniffing canines, the vapor sensing technique has been applied for explosive detection. Vapor sensing detectors sample the explosive molecules volatilized from bombs or landmines, and process the odor signals to identify and locate the bombs. Unlike metal detectors and ground penetrating radars, vapor detection is an unambiguous detection technique that searches for explosives inside the bombs [3]. However, vapor sensing detectors have difficulty in finding bombs with tightly sealed packages that have very few escaping explosive molecules. In short, aforementioned explosive detection schemes all have some drawbacks to prevent them from realizing an on-line, stand-off and portable explosive detection system in field applications [4], [5]. On the contrary, Nuclear Quadrupole Resonance (NQR) is a radio frequency technique that is highly sensitive to the chemical nature of certain isotopes in explosive materials, which makes NQR an attractive option for realizing unambiguous explosive detection systems.

In the past few decades, nuclear resonance technologies have been developed towards explosive detection applications. Nuclear magnetic resonance (NMR) and NQR based detectors are two main trends that the researchers are focusing on. Many remarkable milestones of NQR research have been achieved since 1970s. Smith [7] successfully showed NQR detection results for cyclotrimethylene trinitramine (RDX) and high melting explosive (HMX). Hibbs et al. [8] managed to build up an NQR-based landmine detection prototype system. An NQR baggage scanner for detecting explosives was presented by Rudakov et al. in [9]. Chemistry researchers, such as Ota et al. [10] and Rudakov et al. [11], focused on developing excitation signal patterns to improve detection performance for some new emerging explosives, such as hexamethylenetetramine (HMT) and hexamethylene triperoxide diamine (HMTD). Other researchers who specialize in signal processing, such as Tan et al. [12] and Somasundaram et al. [13], investigated the algorithms for NQR signal post-processing in order to enhance detection performance. However, all of the above accomplishments were initiated from the laboratory perspective. These detection systems, which exist in the form of stationary laboratory demonstration systems, either need high power consumption to achieve high accuracy, or have bulky-sized electrical sections and data processing platforms. Although some NMR miniature systems have been developed in recent years [18], [19], there is no compact sized NQR system that has been reported so far.

In view of limitations of the existing explosive detection systems, we propose an NQR-based explosive detection system

Manuscript received July 15, 2013; revised September 24, 2013; accepted October 2, 2013. Date of publication October 9, 2013; date of current version December 5, 2013. The associate editor coordinating the review of this paper and approving it for publication was Dr. M. R. Yuce.

X. Zhang, S. Balkır, and M. W. Hoffman are with the Department of Electrical Engineering, University of Nebraska - Lincoln, Lincoln, NE 68588 USA (e-mail: xzhang2@huskers.unl.edu; sbalkir@unl.edu; mhoffman1@unl.edu).

N. Schemm was with the Department of Electrical Engineering, University of Nebraska - Lincoln, Lincoln, NE 68588 USA. He is now with Texas Instruments Incorporated, Dallas, TX 95243 USA (e-mail: nathan.schemm@huskers.unl.edu).

Color versions of one or more of the figures in this paper are available online at http://ieeexplore.ieee.org.

Digital Object Identifier 10.1109/JSEN.2013.2285177

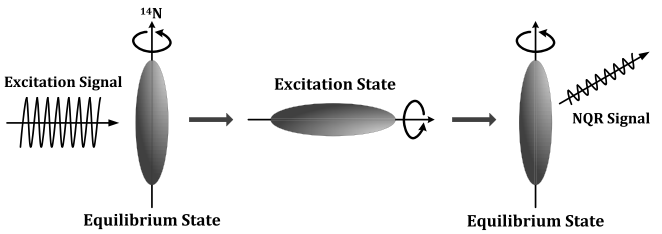

Fig. 1. Illustration of NQR signal excitation.

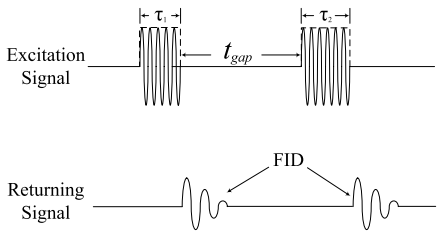

Fig. 2. Illustration of the NQR signal in the time domain.

solution featuring a compact size and low power consumption. The contributions of this work include:

1) A novel Class-D type power amplifier (PA) circuit which is customized for NQR excitation signal generation.
2) A new power multiplexer structure that cooperates with the proposed PA.
3) An integrated low noise amplifier (LNA) based on infinite input impedance power matching.
4) An advanced digital signal processor (DSP) based compact computation platform for NQR signal processing that further shrinks the system volume.

The rest of this paper is organized as follows. The NQR technology background is briefly reviewed in Section II. Section III presents an overview of the proposed NQR detection system with a system-on-chip solution. Section IV describes the novel Class-D PA scheme. A power multiplexing mechanism is proposed in Section V. Section VI and Section VII explain the detailed circuit design and signal processing scheme, respectively. Section VIII presents hardware implementation and shows experimental results on HMT samples. This work is concluded in Section IX.

II. NQR Technology Background

NQR detection is a technique that utilizes the interaction between the electric quadrupole moment of the nucleus and the surrounding electric field gradient (EFG). Thus, it only works for the nuclei that have quadrupole moments. In other words, the spin number I of the nuclei have to be greater than $1/2$. Coincidentally, most of the explosive substances, such as 2,4,6 trinitrotoluene (TNT), RDX, HMTD, etc., are typically rich in ^{14}N (nitrogen) nuclei with $I = 1$. Therefore, NQR is highly amenable to explosive detection.

The NQR frequency is highly sensitive to the distributions of electrons and other nuclei around the nucleus. Hence, the NQR frequency is unique for each explosive substance [14]. According to the literature record [15], the NQR technique has been used on more than 10 thousands of substances for around 30 types of nuclei. No identical NQR frequencies have been found. NQR frequencies of explosive substances usually locate in the range from 500kHz to 6MHz.

As shown in Fig. 1, the ^{14}N spins transit from the equilibrium energy level to the excitation energy level after the excitation signal is applied. The excitation signal is a high power RF pulse which has the pulse width τ. This RF pulse is driven into a coil that surrounds the sample to induce an oscillating magnetic field, denoted as $\mathbf{B}_1$. The magnetic field rotates the ^{14}N spin direction by a conceptual angle α, which is known as the flip angle. α is proportional to $\mathbf{B}_1$ and τ:

$$\alpha = \gamma \mathbf{B}_1 \tau \tag{1}$$

where γ is the gyromagnetic ratio. For ^{14}N, γ is equal to $1.932 \times 10^7 rad\ s^{-1}\ T^{-1}$. Then, the ^{14}N spins precess back to the equilibrium energy level which introduces a decaying RF signal on the same coil or a secondary receiving coil. This decaying RF signal is often called the free induction decay (FID) signal. The time constant by which the sample returns back to the equilibrium state is called *Spin-lattice relaxation time*, denoted as T_1. Note that the decaying time of FID signals is much shorter than T_1. Due to the imperfection of the crystal lattice in the sample and the variation of the temperature distribution throughout the sample, the NQR frequencies of the different ^{14}N spins will be slightly different from each other. Therefore, the actual NQR signals distribute in a very narrow band instead of in a single tone. When the ^{14}N spins precess after the RF pulse is applied, the small frequency differences from different spins lead to phase differences between the signals which make them add up incoherently and eventually cancel out, which occurs much earlier than the sample actually returns to the equilibrium state. The time constant for FID decaying is denoted by T_2^*. The intensity of the NQR signal depends on the flip angle α. Intuitively, the highest NQR signal level can be reached when $\alpha = 90°$. But in real experiments, the results show that the highest NQR signal level is seen when $\alpha = 119°$ [6]. Even with optimized α, the returning NQR signal for one excitation RF pulse is still very weak so that the signal-to-noise ratio (SNR) is too low to make an accurate detection decision. Therefore, most NQR explosive detection systems actually perform the detection by repeating the detection cycles for many times. They utilize RF pulse sequences with certain patterns (multiple RF pulses with the same frequency, sometime different pulse widths) to excite the nuclei of interest. The resultant NQR signals are captured in the time intervals between the RF pulses. The length of the time intervals is denoted as t_{gap}, as shown in Fig. 2. The captured NQR signal during each time interval is called one segment of the whole NQR detection. Then, all the segments are averaged to increase the SNR [6]. In this way, detection accuracy of the systems is improved accordingly.

III. Overview of the Proposed NQR-Based Explosive Detection System

The proposed NQR-based explosive detection system is illustrated by the block diagram shown in Fig. 3. Similar to most explosive detection systems, it consists of a transmitter section, a probe and a receiver section.

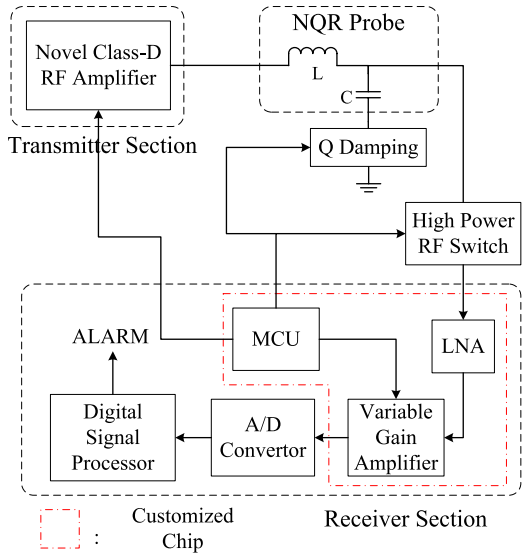

Fig. 3. Block diagram of the proposed NQR based explosive detection system.

The transmitter section performs the task of applying on-off keyed and amplified RF signals as a sequence of excitation pulses to the NQR probe. In traditional NQR detection systems [16], this section is constructed based on an analog RF amplifier. Therefore, all of the auxiliary modules, such as the RF oscillators, RF pulse sequence synthesizers and logic controllers, have to use the circuits working in the analog domain. This type of configuration not only leads to a bulky size and high hardware cost, but also, more importantly, needs high power consumption owing to the low efficiency of analog RF amplifiers. For NQR detection, the pulse width of the excitation signal determines the excitation bandwidth. A shorter pulse width leads to wider excitation bandwidth [17]. From Eq. (1), it can be seen that to achieve the same flip angle, a short pulse width τ needs a high power RF pulse excitation signal to generate high $\mathbf{B}_1$. Therefore, high power efficiency of the PA circuit is desired for the wide bandwidth NQR excitation. In this design, a novel Class-D type PA is proposed to simplify the control scheme and enhance the power efficiency of the transmitter section in favor of portability.

The NQR probe is, in essence, an LC tank which has a resonant frequency that can be tuned to the NQR frequencies of different substances. For system simplicity, the same probe is shared between the transmitter and receiver sections. By driving a high power RF signal into the probe, the inductor, denoted as L in Fig. 3, generates the oscillating magnetic field during the transmitting phase to excite the sample at its specific NQR frequency, and collects the returning NQR signal from the sample afterwards. In order to achieve high excitation power and high detection sensitivity, a high Q factor of the NQR probe is preferred. On the other hand, a short recovery time of the probe is necessary for measuring the FID signal because it appears right after the transmission. Since the recovery time is proportional to the Q factor, a low Q factor is desired after the transmission. In this design, a Q damping circuit is added to promptly switch the probe to a lower Q factor for quickly decaying the residue ringing at that moment; and then switch back to the higher Q value for detection and next transmission period.

The receiver section starts with a low noise amplifier (LNA) to amplify the returning NQR signal while constraining the noise figure (NF) of the whole receiver chain. In this design, a so-called infinite input impedance power matching scheme [18] is adopted for the LNA in order to achieve a low NF. As the LNA can be damaged by the high power RF signal during the transmitting phase, an RF switch is added to isolate the transmitting signal. During the receiving phase, to detect the inherently weak NQR signal, this RF switch is required to have small additive attenuation as well as low noise contribution. A PIN diode based RF switch is employed to satisfy these requirements. Following the LNA, a variable gain amplifier (VGA) further enlarges the NQR signal before it being delivered to the analog-to-digital converter (ADC). The gain of the VGA can be tuned to adequately utilize the dynamic input range of the ADC, as well as to prevent the signal from saturating the input stage of the ADC. Then, the NQR signal is digitized by the ADC and sent to a DSP for downstream processing. Using a DSP as the data processing platform is another advantage introduced by this design, compared to the traditional detector configurations wherein bulky personal computers (PCs) or other comprehensive computation units are employed. Although PCs can provide versatile programmability and extensive computation power, the state-of-the-art DSPs possess specialized computational structures to cope with NQR data analysis in the frequency domain while maintain ultra small volume and low power consumption.

The overall detection procedure is coordinated by a microcontroller (MCU) that is integrated with the LNA and VGA on the same customized IC designed by the authors. First, the MCU starts the transmitter control logic with synthesizing the NQR frequency and programming the RF pulse sequence. While keeping a high Q factor of the NQR probe, it shuts off the RF switch, and commands the Class-D PA to generate a high power stimulus signal to the NQR probe. After each transmitted RF pulse, the Q damping circuit is triggered to lower the Q factor of the probe for quickly damping the residual power. When the Q factor is switched back to the higher value, the RF switch is turned on, and the receiving chain starts to collect data of this segment and restore them for DSP processing. The DSP performs data processing in parallel with data collection to reduce the overall response time.

The whole system is implemented in hardware, and the photo of the prototype system is shown in Fig. 4. The details of implementation are described in the following sections.

IV. Novel Class-D Voltage-Switching Power Amplification Scheme

During the transmission period, RF pulses are amplified to a high power level and driven into the NQR coil to generate the oscillating magnetic field $\mathbf{B}_1$. An ideal square RF pulse has zero rising up time t_{start} and zero decaying time t_{stop}. The width of the RF pulses τ_i is an important design variable that controls the flip angle of the nucleus spins, as indicated in Eq. (1). In reality, as NQR probes usually have a high Q

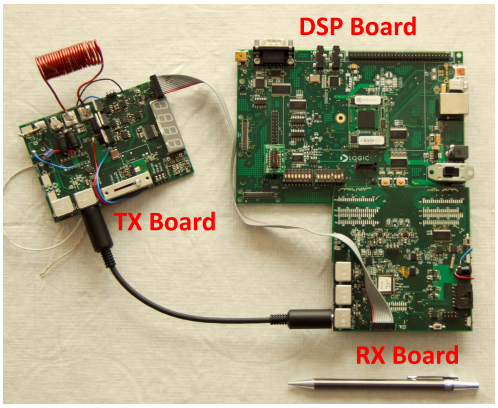

Fig. 4. Photo of the prototype system.

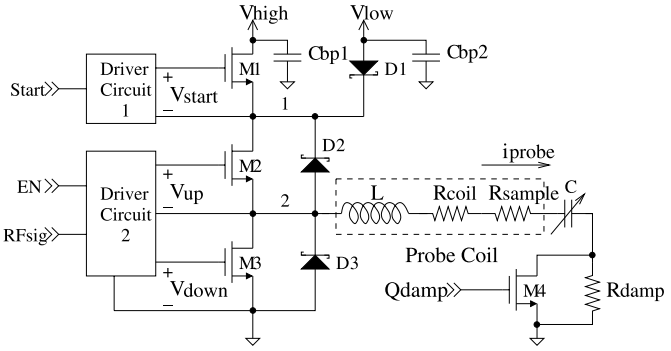

Fig. 5. Class-D voltage-switching PA with fast-start and fast-stop functions [21].

factor in the range of $80 \leq Q \leq 200$ [6], the real radiated RF pulses have long t_{start} and t_{stop}. A long t_{start} will significantly shorten the width of the real radiated RF pulses, thus affecting the precision of flip angle controlling. Meanwhile, as FID signals are collected right after the RF pulses, the residual oscillating stimulus signals, caused by t_{stop}, become interference for the returning RF signals. Therefore, fast-start (short t_{start}) and fast-stop (short t_{stop}) functions for the PA will greatly improve the control and detection precision of the NQR system. In addition, to design a PA for portable systems, high power efficiency is certainly desired.

In order to address the aforementioned design requirements, a novel Class-D voltage-switching PA circuit is proposed in this design. High power efficiency is the main advantage of this PA scheme thanks to its switching nature. In addition, this PA is equipped with the circuits that realize fast-start and fast-stop functions to facilitate NQR detection. The design details of this part of work have been published by the authors in [21]. In this context, a brief review is given for convenience and consistency.

Fig. 5 illustrates the simplified circuit of the proposed PA. MOSFETs M_2 and M_3 combining the diodes D_2 and D_3 are configured as two bidirectional switches. The switches are turned on and off alternately with the resonant frequency f_o to achieve high-efficiency power delivery to the series LC NQR probe. M_1 and D_1 are added to switch the voltage supply V_1 to realize the fast-start function. In order to reduce t_{start}, a higher amplitude signal is driven into the LC tank at the start. At the beginning of the transmission period, M_1 is turned on to switch V_1 to V_{high}, a higher-value power supply, to shorten t_{start}. Once the power inside the NQR coil reaches the desired level, M_1 is turned off so that V_1 is switched to V_{low} for maintaining the oscillating power. The fast-stop function can be achieved by manipulating the ending procedure in two steps. First, both of M_2 and M_3 are shut off. At this moment, the residual energy inside the NQR coil is so high that it can turn on D_2 and the body diode of M_1 to dump the energy back to C_{bp1} while $iprobe < 0$. This mechanism clamps the voltage amplitude of oscillation in the RF probe in a very short time, usually 2-4 cycles of the oscillating signal. The major part of the residual energy is dissipated through this step. Then, M_4 of the Q-damping circuit is turned off, R_{damp} depletes the rest of the residual energy to further reduce t_{stop}.

V. Power Multiplexing and Matching Mechanism

Generally, parallel LC tank type RF probes are used for NQR signal detection during the receiving period. However, during the transmitting period, in order to realize low power operation, a series LC tank type NQR probe is required by the proposed Class-D PA circuit. Therefore, a power multiplexing strategy is designed to coordinate the transmitting section and receiving section. Meanwhile, inspired by [18], an infinite impedance power matching mechanism is employed along with the NQR probe to achieve low noise detection.

A. Infinite Impedance Power Matching Scheme

As NQR frequencies of explosive materials range from 500kHz to 6MHz, the wavelengths of NQR signals (from 50m to 600m) are substantially longer than the scale of the system. Therefore, the lumped circuit model is used to analyze the power matching mechanism.

Among the laboratory NQR systems, standard LNAs with 50Ω input impedance are often used to provide initial amplification for NQR signals as they are off-the-shelf devices. Accordingly, an NQR coil is often equipped with a matching network which transfers the output impedance of the NQR probe to 50Ω to pair up with the general LNAs. A widely used matching network along with the NQR coil is shown in Fig. 6(a). C_1 and C_2 construct a L–section matching network to transfer the NQR probe output impedance for impedance matching. A signal source V_{sig} is used to represent the NQR signal picked up by the NQR coil. Two main noise sources determine the noise power at the receiver. One is caused by the parasitic resistance of the coil; the other is the noise from the detection environment. Without loss of generality, the noise is modeled by $\sqrt{\overline{V_{noise}^2}}$. If perfect matching is achieved at the NQR signal frequency ω_o, the equivalent circuit in Fig. 6(a) can be used to derive the signal power and the input noise power for the LNA.

First of all, $\sqrt{\overline{V_{noise}^2}}$ and V_{sig} are combined to find V_2:

$$V_2 = \frac{(V_{sig} + \sqrt{\overline{V_{noise}^2}})}{1 + \frac{C_1}{C_2} + j\omega RC_1 - \omega^2 LC_1}. \quad (2)$$

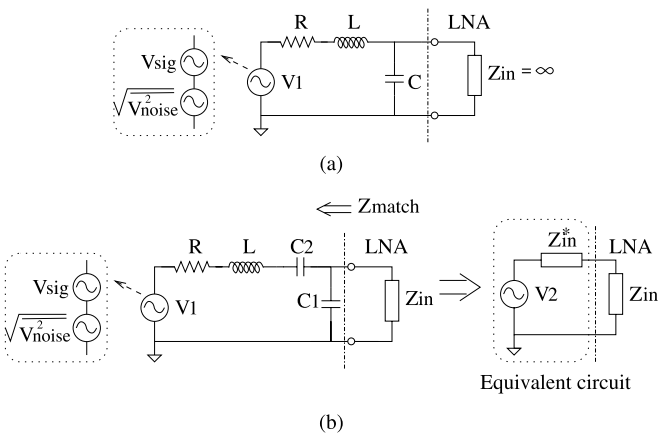

Fig. 6. Comparison of the power matching schemes. (a) 50Ω matching scheme. (b) Infinite Z_{in} matching scheme.

Hence, by letting $\sqrt{\overline{V_{noise}^2}} = 0$, the input signal to the LNA is:

$$|V_{sig\_in}| = \left|\frac{1}{2}V_2\right|_{\sqrt{\overline{V_{noise}^2}}=0} = \frac{\frac{1}{2}|V_{sig}|}{\sqrt{(1+\frac{C_1}{C_2}-\omega_o^2 LC_1)^2+(\omega_o RC_1)^2}}. \quad (3)$$

By letting $V_{sig} = 0$, the input noise to the LNA is:

$$\left|\sqrt{\overline{V_{n\_in}^2}}\right| = \left|\frac{1}{2}V_2\right|_{V_{sig}=0} = \frac{\frac{1}{2}|\sqrt{\overline{V_{noise}^2}}|}{\sqrt{(1+\frac{C_1}{C_2}-\omega_o^2 LC_1)^2+(\omega_o RC_1)^2}} \quad (4)$$

When $w = w_o$, the L–section matching network should be able to transfer the coil impedance $R + j\omega L$ to $Z_{match} = Z_{in} = 50\Omega$. To that end, C_1 and C_2 should be [20]:

$$C_1 = \frac{1}{\omega_o Z_{in}}\sqrt{\frac{Z_{in}-R}{R}} \quad (5)$$

$$C_2 = \frac{1}{\omega_o^2 L - \omega_o\sqrt{R(Z_{in}-R)}}. \quad (6)$$

Substituting Eq. (5) and Eq. (6) into Eq. (3) and Eq. (4), we have

$$\left|V_{sig\_in}\right| = \frac{1}{2}\sqrt{\frac{Z_{in}}{R}}|V_{sig}| \quad (7)$$

$$\left|\sqrt{\overline{V_{n\_in}^2}}\right| = \frac{\frac{1}{2}|\sqrt{\overline{V_{noise}^2}}|}{\sqrt{\frac{R^2}{Z_{in}^2}+\frac{(Z_{in}-R)R}{Z_{in}^2}}} = \frac{1}{2}\sqrt{\frac{Z_{in}}{R}}|\sqrt{\overline{V_{noise}^2}}|. \quad (8)$$

Let us now consider the power matching scheme shown in Fig. 6(b), wherein the LNA is customized to have infinite input impedance. The input of the LNA is directly connected to the resonant capacitor C. Similarly, the input signal of this LNA can be derived as

$$V_{sig\_inf\_in} = \frac{V_{sig}}{1+j\omega RC-\omega^2 LC} \quad (9)$$

and the noise is

$$\sqrt{\overline{V_{n\_inf\_in}^2}} = \frac{\sqrt{\overline{V_{noise}^2}}}{1+j\omega RC-\omega^2 LC}. \quad (10)$$

Unlike the 50Ω matching network, Fig. 6(b) only contains one resonant capacitor — C. When $\omega = \omega_o$, $\omega_o^2 LC = 1$. Therefore, we have

$$\left|V_{sig\_inf\_in}\right| = \frac{|V_{sig}|}{\omega_o RC} = Q|V_{sig}| \quad (11)$$

$$\left|\sqrt{\overline{V_{n\_inf\_in}^2}}\right| = \frac{|\sqrt{\overline{V_{noise}^2}}|}{\omega_o RC} = Q|\sqrt{\overline{V_{noise}^2}}|. \quad (12)$$

Comparing Eq. (7) to Eq. (11) and Eq. (8) to Eq. (12), both of the two passive RLC networks, (L, C_1, C_2) and (L, C), provide certain gains to the signal as well as the noise. But the infinite impedance matching scheme has much higher gain than the 50Ω matching scheme. The gain from the passive networks helps improve the NF. By definition, the NF of the LNA is the ratio between the total output noise power and the portion of output noise power contributed by the input noise of the circuit:

$$NF = \frac{P_{noise\_out}}{A^2\ P_{noise\_in}} = \frac{A^2G^2\overline{V_{n\_in}^2}+A^2\overline{V_{n\_LNA\_in}^2}}{A^2G^2\overline{V_{n\_in}^2}} = 1+\frac{\overline{V_{n\_LNA\_in}^2}}{G^2\overline{V_{n\_in}^2}} \quad (13)$$

where A is the gain of the LNA; G represents the gain of the passive network; and $\overline{V_{n\_LNA}^2}$ denotes the input referred additive noise power of the LNA. From Eq. (13), we can see that two design options can be adopted to minimize the NF. The first option is to minimize the additive noise from the LNA. This part of work is discussed in Section VI-A. The other option is to maximize G. Therefore, assuming the LNA for each case has similar additive noise power, and $\overline{V_{noise}^2}$ is at the same level for both matching networks, since the infinite impedance matching scheme has a much higher gain than the 50Ω matching scheme, the NF of the LNA with infinite impedance matching is much lower.

Furthermore, tuning the 50Ω matching network requires changing two design variables C_1 and C_2 for a specific NQR frequency, whereas infinite impedance matching only needs to change one resonant capacitor C. From the perspective of design complexity, the infinite impedance matching is more favorable.

B. Power Multiplexing Strategy

In order to benefit from both the Class-D PA, which requires a series LC network, and the infinite impedance power matching scheme, which requires a parallel LC network, there should be two switchable configurations for connecting the NQR probe coil and resonant capacitor. To fulfill this function, a power multiplexing strategy is proposed.

Fig. 7 shows the output stage of the Class-D PA and NQR probe. During the transmitting period, $M1$ and $M2$ is turned

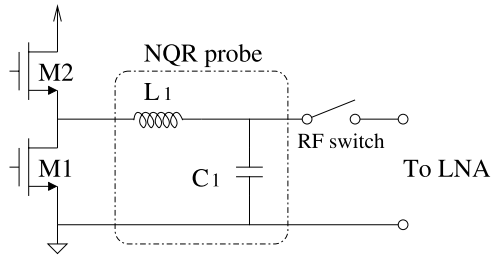

Fig. 7. The Class-D PA output stage with the NQR probe.

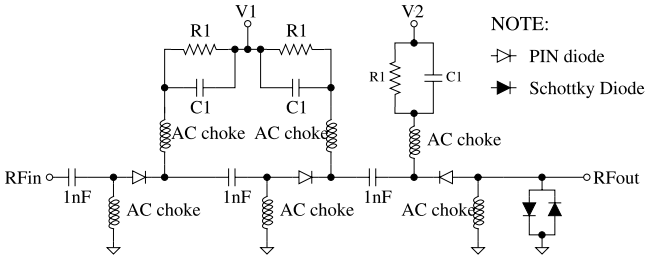

Fig. 8. Three stage PIN diode RF switch.

on alternately to maintain the transmission power while the RF switch is kept open. When the receiving period starts, $M1$ is turned on while $M2$ is shut off such that the NQR probe is connected in a parallel LC tank manner. Now the RF switch is closed to conduct the signal to the LNA. When $M1$ is turned on to construct the parallel-LC-tank NQR probe, this NMOS can be modeled as a resistor in series with the NQR probe. Its resistance is equal to R_{on}, the on-resistance of $M1$. Usually, $M1$ is chosen to have very small R_{on} value (tens of $m\Omega$) such that the Class-D PA can achieve high power efficiency. On the other hand, the series resistance of the coil is generally greater than hundreds of $m\Omega$. Therefore, $M1$ only contributes around 10% additional series resistance. In addition, the MOSFET in the Q damping circuit ($M4$ in Fig. 5) will contribute some series resistance. Compared to $M1$, $M4$ is chosen to have even smaller R_{on} (several $m\Omega$) as it does not have switching speed concern. As a result, the Q factor of the NQR probe is compromised to 10% less of its original value. $M1$ and $M4$ will certainly increase the thermal noise level. When they are fully turned on, the thermal noise of $M1$ and $M4$ is determined by their R_{on}. The series resistance of the coil is still the dominant noise source for NQR detection. Therefore, this NF degradation is tolerable.

C. PIN Diode Based RF Switch

The RF switch is playing a key role through the whole NQR detection process. On one hand, the RF switch needs to have high isolation capability so that the high transmission power efficiency can be sustained. Meanwhile, the sensitive receiver-side circuits also need to be protected from high transmission signal power. On the other hand, the RF switch must exhibit low signal degradation as the NQR signals are inherently weak and very vulnerable to any disturbance.

During the transmitting period, the NQR probe is configured as a series LC tank with a very high Q factor, which can reject the harmonics generated by the Class-D amplifier. The RF switch is connected in the middle point of the LC tank, as shown in Fig. 7, and it does not see the harmonics from the Class-D amplifier. In another word, the RF switch only sees the heavily attenuated harmonics that will not damage the receiver circuit. Therefore, a narrow rejection band RF switch such as a quarter-wave switch, or a wide rejection band RF switch such as a PIN diode based switch, can be used.

Traditional NQR lab equipments often employ quarter-wave switches, which has a simple structure and does not require any control circuit. Its low additive noise benefits the detection accuracy. However, for portable explosive detection NQR systems, it is not a practical choice as it normally requires a long transmission cable. For example, for a 4MHz signal, the length of the transmission cable is $\lambda/4 \approx 19m$. Moreover, different explosive materials require different cable lengths, as they have different wavelengths, which largely complicates the system design.

PIN diodes are semiconductor devices which consist of three layers: a high resistive intrinsic I layer in between highly doped P-type layer and N-type layer [22]. The I layer provides high isolation between the P and N layers so that the capacitance between the P and N terminals is very low (around a few pF). A more interesting characteristic of PIN diodes is that as charging and discharging I layer requires a certain amount of time (usually around tens of μS), high power AC signals can be switched on and off with a low power DC biasing control signal. Moreover, when a PIN diode is forward biased, it has low additive resistance whose value depends on the DC bias current. Generally, with a $100mA$ DC forward biasing current, the resistance can drop to less than 1Ω. This feature leads to low insertion loss as well as low additive noise. Especially with the infinite impedance power matching scheme, the RF switch is between the NQR probe and LNA with infinite input impedance. The noise power contributed by the NQR coil is already amplified by the passive network. The noise caused by the PIN diode is much smaller than the noise power from the passive network, and therefore adds a negligible portion to the total noise going to the LNA. Regarding the insertion loss, since the LNA has very large input impedance, and the NQR signal current flowing through the RF switch is very small, the insertion loss caused by the PIN diode is also negligible.

Compared to quarter-wave switches, PIN diode switches have some drawbacks: 1) they require extra control and driving circuits to support the PIN diodes; 2) they consume power during turn-on state as a DC bias current is needed to provide low signal attenuation. Despite the drawbacks, the advantages of PIN diode switches are more remarkable: 1) they can be integrated in a compact volume; 2) they have a universal setup for all explosive materials.

In this design, a 3-stage PIN diode based switch is employed. Its simplified schematic is shown in Fig. 8. The first two stages are operating on a high voltage ($V1$ in Fig. 8) during off-state. Since the voltage amplitude of the oscillation inside the NQR probe during the transmission period can easily reach 500V, $V1$ must be able to be adjusted up to 100V. Two normal RF diodes are added at the receiver side

to guarantee the protection for the LNA. The third stage is switched by a low voltage, $V2$ in Fig. 8, to make sure those two RF diodes are well isolated from the NQR probe during high power transmission. During the receiving period, all PIN diodes are forward biased with a 100mA DC current, which means $V1$ and $V2$ needs to be pulled down to a negative value. $R1$ in Fig. 8 provides the current limitation. When the PIN diodes are being turned on, i.e. the driving signal is switching from positive to negative, $C1$ provides a low impedance path to reduce the turning-on time for the PIN diodes. Test results show that this 3-stage PIN diode switch can provide up to 75dB isolation with 20 μs turning-on time.

VI. Customized CMOS Mixed-Signal IC

Due to the fast evolving CMOS mixed-signal design technology, the mainstream idea of designing compact circuit systems nowadays is to integrate multiple function units, which even cross digital and analog signal domains, into one single chip. In this work, we also take this advantage to further reduce the volume and cost of the system by designing and fabricating a customized CMOS IC. This chip is designed with 0.18 μm CMOS process. It consists of an LNA, a VGA and an MCU. The LNA with conceptually infinite input impedance is designed to realize the power matching scheme discussed in Section V-A. The VGA that follows the LNA provides amplification for NQR signals. The gain of the VGA is tuned by the DSP to form an auto gain control (AGC) feedback loop. The main purpose of the AGC is to fully utilize the input dynamic range of ADC, as well as to keep the ADC from being saturated. The MCU is responsible for generating control logic to coordinate the transmitting and receiving sections.

A. LNA Design

CMOS-based amplifiers can have very large input impedance as their active devices, MOSFETs, are voltage controlled. More specifically, the input end can be connected to the gates of MOSFETs which ideally have no DC current path except a small amount of gate leakage current. For AC signals, when MOSFETs are in the saturated region, which normally is the case for CMOS amplifiers, the gate parasitic capacitor is usually less than 1pF [23] even for large size MOSFETs. Therefore, compared to the resonant capacitor of the NQR probe, the input impedance of CMOS-based amplifiers can be considered a very high value which satisfies the infinite input impedance power matching scheme. The simplified schematic of the LNA circuit is shown in Fig. 9. The two input ends of the LNA are connected to the two sides of the NQR probe via the RF switch. From the discussion in Section V-A, in order to minimize the NF of the system, additive noise from the LNA should be minimized. In the NQR frequency range, $1/f$ noise is still comparable to thermal noise for the CMOS technology. Hence, PMOS is used as the input stage to have smaller $1/f$ noise as PMOS generally has less $1/f$ noise ($1/3$ of NMOS's with the same bias condition and size). The two input PMOS transistors are assigned with a large area, $2\times 800\mu m\times 0.36\mu m$ to suppress $1/f$ noise. In addition, a large bias current, 2mA, is driven through the input pair to reduce the thermal noise.

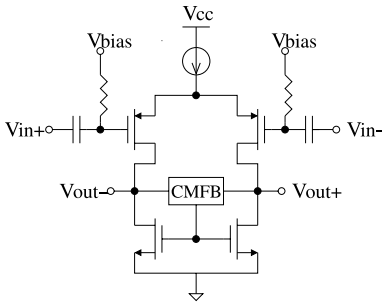

Fig. 9. Differential low noise amplifier (CMFB: common mode feedback circuit).

The differential structure is used to cancel the common-mode noise that is prevalent for sensor circuits. The gain of the LNA is designed to be $30-40$dB. If the passive network is taken into account for calculating the NF, this LNA can achieve a NF as low as $< 1dB$.

The LNA is followed by another open loop preamplifier that has a $30dB$ fixed gain and low additive noise to further improve the NF of the whole system. Then, NQR signals go through the VGA with a gain tunable range from 0dB to 72dB. The VGA consists of four cascaded stages. Each stage is realized by an opamp-based close loop amplifier. As well known, close loop amplifiers have high linearity and accurate controllable gain. Each of the VGA stages has two gain control bits that tune the gain between 0dB to 18dB ($Gain = 0 \sim 8$).

B. MCU

A 16 bit Reduced Instruction Set Computing (RISC) core is integrated on the chip to fulfill the logic control for the NQR system. As the core is dedicated to control sequence and timing generating, its design is greatly simplified. Only a small instruction set consisting of 28 instructions has been implemented. Communication interfaces, such as SPI, UART and I2C, are included as peripherals on the MCU to facilitate the communication between the MCU, ADC and DSP, as well as the programming for each module. Timing control for the system is mostly achieved by a hardware timer on the MCU. The working frequency of the core can reach as high as 60MHz. All the instructions can be executed in a few clock cycles. Therefore, it is powerful enough to handle the control work for the NQR system. The design details of the MCU can be found in [24].

VII. System Control and Signal Post-Processing

Different parts of an NQR detection system need to be coordinated to achieve the NQR signal detection. With the new Class-D power amplification scheme and power multiplexing and matching network, the control logic pattern must be customized and optimized for the proposed system. Besides, owing to the requirements of on-line and real-time detection, NQR signal data should be collected instantly and be processed immediately after collection. Hence, fast processing speed and powerful computation capability are desired. As the detection environment changes from case to case, a certain level of programmability is also necessary. In addition, the

power consumption and size constraints for portable systems should be enforced for this portion of system. As aforementioned, a customized MCU is used to provide logic control; and a *C*6000 series DSP from Texas Instruments is employed for data collection and processing. In this section, some key design considerations are described in details.

A. NQR Data Collection and Processing

After sufficient amplification provided by the LNA and VGA, NQR signals are digitized by the ADC for further processing. In the prototype NQR detection system, a *C*6748 evaluation board is utilized to verify the feasibility of using this DSP as the data processing platform. Some key features of *C*6748 differentiate it from other candidates [25]. First, with up to 450MHz working frequency, it provides very powerful computation capability as well maintain low power consumption. Under typical working conditions, it only consumes 426mW according to [26]. Second, *C*6748 has a high speed memory controller that supports 16-Bit DDR2 SDRAM with 512MB address space. The large memory space is highly desired for NQR data collection, especially for multiple pulse sequence detection. Third, *C*6748 is furnished with a high speed universal parallel port (UPP) peripheral through which DSPs can directly communicate with high sample rate data converters. With the large amount of data that needs to be transferred from the ADC, the UPP is the most essential feature of *C*6748 for NQR data collection.

At the beginning of each receiving cycle, the DSP is interrupted by a cue signal from the MCU indicating that a new data segment needs to be transferred. Upon being interrupted, the CPU enables the Direct Memory Access (DMA) to get ready to receive the data. Then, the data is transferred through the UPP and DMA to the external memory directly. In this way, the CPU is able to process the previously received data in parallel. The overall detection time is reduced.

B. Logic Control for the NQR System

From the discussions above, the logic control for the whole system can be summarized as: 1) Class-D PA control that involves fast-start, fast-stop and oscillating signal generation; 2) power multiplexing control that includes PIN diode switch control for receiving and transmitting periods; 3) ADC, VGA and DSP control involving the inter-communication and enable-disable control. 4) NQR stimulus signal pulse width control and multiple pulse sequence control. The logic control does not only guarantee the working sequence of different functional units, but also, more importantly, adjust the timing between control events. All the clock signals, such as the NQR frequency clock for the Class-D PA, the ADC sampling clock, and the clock for timing control circuit are synchronized.

Fig. 10 demonstrates the simplified logic sequence. For each receiving and transmitting cycle, the process can be divided into 8 timing events. ENb and $NMOS\_ctrl$ are the control signals for the Class-D PA switching power stage. When ENb is low, NMOS of the power stage is driven by $NMOS\_ctrl$, and PMOS is driven by the inverted version of $NMOS\_ctrl$. $Startup$ is the control signal to switch the power supply for the Class-D PA to realize fast-start function. $Q\ Damping$ turns on the Q damping circuit for fast-stop function. SW_ENb and SW_EN turns on and off the PIN diode switch. td, the dead time between the transitions of SW_ENb and SW_EN is introduced to prevent the shoot-through in the PIN diode driver circuit. ADC_EN is the enable signal for the ADC. DSP_cue is the signal for the DSP indicating that the receiving period is started. The ADC is enabled on time 3, before DSP starts collecting data, to make sure the initiation process of the ADC is finished. $t2$ is the pulse width of the NQR stimulus pulse that controls the flip angle of the nuclei, as explained in Section II. $t6$ and $t7$ can be changed to capture different portions of NQR signals.

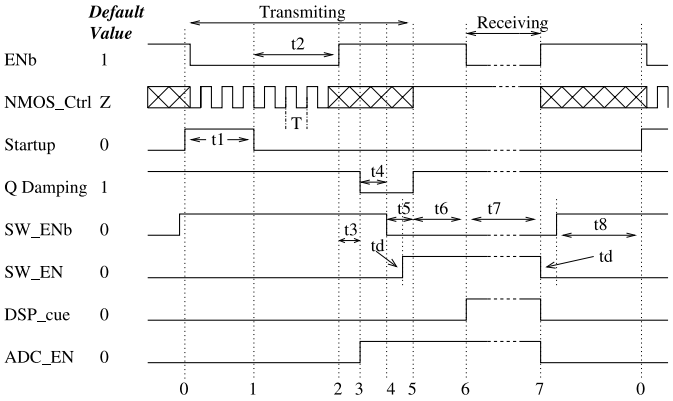

Fig. 10. Simplified control logic waveforms.

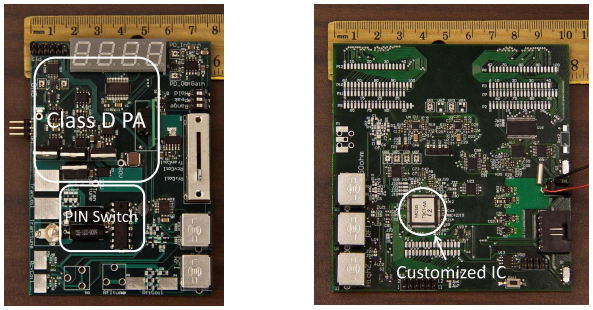

(a) (b)

Fig. 11. (a) TX and (b) RX boards.

VIII. Hardware Implementation and Experiment Results

The proposed portable NQR based explosive detection system is implemented to verify its feasibility. The prototype system consists of two main sections, receiving (RX) and transmitting (TX). In order to improve noise isolation and coupling blockage, the RX and TX sections are designed as two separate boards, which are shown in Fig. 11(a) and (b), respectively. The size of the TX board is $10.6cm \times 7.6cm$. It contains the Class-D PA, PIN diode based RF switch, and power matching circuit for the NQR probe coil. Control signals for the TX section are provided by the RX board. The size of the RX board is $10.2cm \times 10.7cm$. The proposed customized IC resides on it with necessary supporting circuits. Fig. 12 is

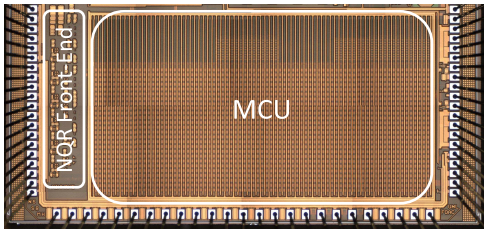

Fig. 12. Customized IC.

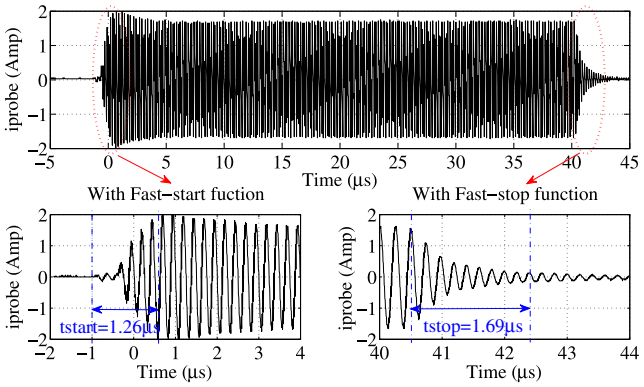

Fig. 13. i_{probe}, t_{start} and t_{stop} with fast-start and fast-stop functions.

the die photo of the customized IC. The total area is $6.55mm^2$, wherein the NQR front-end occupies $0.45mm^2$. The ADC on the RX board has the sample rate up to 80MHz with 12 bit resolution. The RX board has a port to communicate with the $C6748$ evaluation board.

A. Class-D PA Test Results

The Class-D PA circuit is tested to evaluate its performance, including startup time (t_{start}), stop time (t_{stop}) and power efficiency (η). In this prototype system, the possible maximum output power of the PA is designed to be 1kW. Since the NQR signal frequencies of the explosives are in the range from 500kHz to 6MHz, the maximum operating frequency of the PA is designed to be 10MHz.

Fig. 13 shows a measured NQR excitation signal with a frequency equal to $4.009MHz$. The pulse width of the excitation signal, τ, is 41 μs. In Fig. 13, i_{probe} is the current through the probe. The NQR coil utilized in this setup has $L = 2.9$ μH and $R_L = 3.5\Omega$ ($Q = 20.9$). With $V_{high} = 40$V and $V_{low} = 10$V, i_{probe} has an amplitude of 1.7A in the steady working condition. M_1 in Fig. 5 is turned on for 1.5μs to fulfill the fast-start function, which leads to $t_{start} = 1.26$ μs. Compared to the startup time without turning on fast-start function, the improvement is significant, 80% less. The measured t_{stop} is 1.69 μs with turning off M_4, which demonstrates 43% improvement comparing to the t_{stop} without turning off M_4.

The measured efficiency of the Class-D PA is around 61% with this NQR coil. Detailed evaluation results of Class-D PA can be found in [21].

TABLE I
POWER CONSUMPTION FOR EACH FUNCTION MODULE

Function Module		P_R (mW)	P_T (mW)	P_I (mW)
RX Board	NQR Front-End	67	1	1
	ADC	308	30	30
	MCU	9	9	9
	Supporting Circuit	188	188	188
	Total	572	228	228
Class-D PA		50	P_{out}/η	50
PIN Switch		1500	3	3
Total		2122	$P_{out}/\eta + 231$	281

P_R is the power consumption in the receiving state.
P_T is the power consumption in the transmitting state.
P_I is the power consumption in the idle state.
P_{out} is the output power that is driven to the NQR probe during transmitting period.
η is the measured power efficiency of the Class-D PA.

B. Power Consumption Analysis of the Prototype System

Other than the compact size, power consumption is also an important aspect for portable applications. Therefore, a power consumption analysis is performed in this section. Referring to Fig. 10, one cycle of the detection action, denoted as T, can be divided into three portions of time for power consumption analysis — transmitting state ($t_1 + t_2$ in Fig. 10), receiving state (t_7 in Fig. 10) and idle state (t_8 in Fig. 10). For the transmitting state, most of the power is dedicated to generating NQR stimulus signals. The Class-D PA is in the operation mode. The MCU provides logic control to the Class-D PA. In the prototype system, to guarantee accuracy and low noise of the NQR clock frequency, a stand-alone synthesizer is applied to generate the clock signal for the Class-D PA. The ADC is set to the low power mode. The PIN diode switch is in off-mode which only has a negligible reverse leakage current, measured less than 10 μA. During the receiving period, the Class-D PA is turned off. The NQR frond-end is enabled to provide amplification to NQR signals. The ADC is enabled and the DSP is in normal operation mode. Meanwhile, the PIN switch is turned on with forward biasing the PIN diodes. To minimize additive noise and insertion loss of the PIN diode switch, the forward DC biasing current should be maximized, but bounded by the current limit of the PIN diodes. In the idle period, which is the time frame between receiving and transmitting, every part is disabled except the MCU. The detailed power consumption characterization is listed in Table I. The total power consumption of the system for each detection cycle P_{system} is:

$$P_{system} = \frac{P_R \cdot t_7 + P_T \cdot (t_1 + t_2) + P_T \cdot t_8}{T}. \qquad (14)$$

C. HMT NQR Signal Detection Using the Prototype System

As hexamethylenetetramine (HMT) is more stable compared to other explosives, it is often used for the NQR equipment testing in the laboratory. In addition, its NQR signal frequency is 3.309MHz at room temperature, which approximately falls

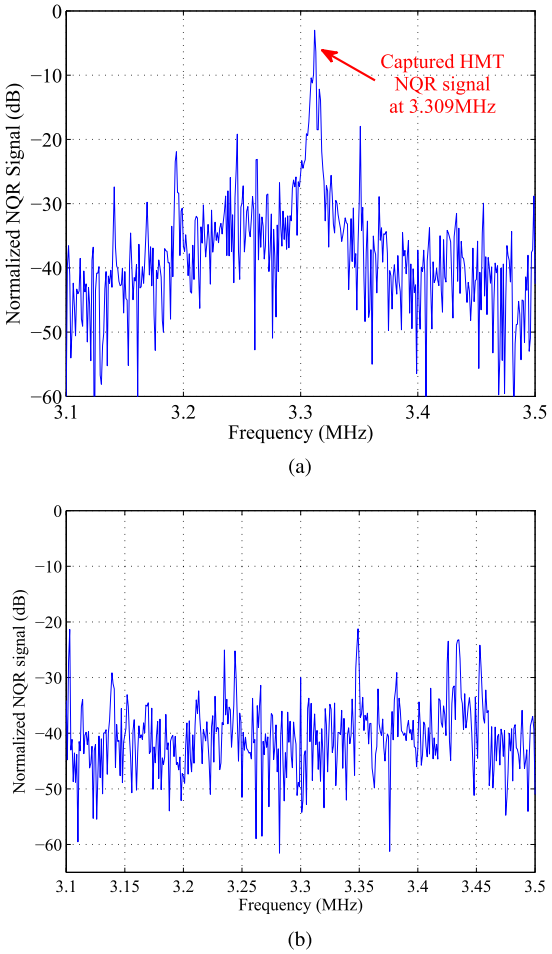

Fig. 14. HMT NQR signal test results. (a) With HMT sample presented. (b) Without HMT sample presented.

on the center point of the explosive NQR signal bandwidth, 500kHz to 6MHz.

A solenoid coil is employed as the probe for HMT NQR signal measurement. The solenoid coil is made of magnet wire that has the diameter equal to 1.6mm. The length of the coil is 44mm with 23 turns, $N = 23$. The diameter of the coil is 16mm. The measured inductance of the coil is $L = 2.6318\mu H$, and the series resistance is $R_s = 0.607\Omega$. At the HMT NQR frequency 3.309MHz, the quality factor of the coil is $Q = 90$. Given the physical size of the coil, the estimated magnetic flux density inside the coil can be derived as $B = \mu Ni/L = 6.72 \times 10^{-4} \cdot i\ T$, where i denotes the AC current driven into the coil. Theoretically, the intensity of a NQR signal reaches its maximum value when the flip angle is equal to 119° [10]. According to Eq. (1), the estimated pulse width which yields 119° flip angle is $\tau = 159/i\ \mu$s. In this experiment, the Root Mean Square (RMS) value of the stimulus AC current is adjusted to be around 4A, which leads to $\tau \approx 40\ \mu$s.

In the real sample test, 5g of the HMT sample is placed inside the solenoid coil. With $i_{rms} = 4.12$A and $\tau = 30\ \mu$s, the maximum NQR signal level can be captured. The sampling frequency is set to 40MHz. The NQR signal is recorded 50 μs after the stimulus pulse ends. For each stimulus pulse, the receiver records 3 ms of the NQR signal from the NQR probe. The interval between two stimulus pulses t_{gap} is 1s. The detection cycle is repeated 100 times. NQR signal segments of 100 receiving cycles are averaged to increase the SNR. The spectrum of the detected HMT NQR signal is shown in Fig. 14(a). To demonstrate the detection behavior of the prototype system, the detected signal spectrum with the identical setup but without HMT sample presented is shown in Fig. 14(b). Comparing Fig. 14(a) and (b), the prototype system can provide an around 40dB SNR with the current setup. The detection function is proven effective. For each detection cycle, the RX board consumes averagely 572mW during the receiving period, and 228mW during the transmitting and idle period. On the TX board, by using $\eta = 60\%$, the Class-D PA consumes averagely 16W during the transmitting period and 50mW during the receiving period and idle period. The PIN diode switch consumes 1.5W during the receiving period and less than 3mW during the transmitting and idle period. In total, the average power consumption of the prototype system for this test setup is 287mW, calculated by using Eq. (14).

IX. Conclusion

A low-power, compact portable NQR based explosive detection system solution has been presented in this work. Several novel structures of the key modules integrated in the proposed detection system are discussed and evaluated in details. These modules, including the Class-D type PA, power multiplexing and matching network, customized IC, and DSP-based signal processing platform, greatly shrink the volume of the system while maintaining low power consumption of the whole detection cycle. Test results of the prototype system prove the effectiveness and feasibility of the proposed solution.

References

[1] N. E. Walsh and W. S. Walsh, "Rehabilitation of landmine victims—The ultimate challenge," *Bull. World Health Org.*, vol. 81, no. 9, pp. 665–670, 2003.

[2] National Research Council, *Existing and Potential Standoff Explosives Detection Techniques*. Washington, DC, USA: National Academy Press, 2004.

[3] J. W. Gardner and J. Yinon, *Electronic Noses and Sensors for the Detection of Explosives*. Norwell, MA, USA: Kluwer, 2004.

[4] L. Theisen, D. Hannum, D. W. Murray, and J. E. Parmeter, "Survey of commercially available explosives detection technologies and equipment 2004," The Nat. Law Enforcement and Correction Technology Center, Nat. Inst. Justice, Rockville, MD, USA, Tech. Rep. 208861, 2004.

[5] J. E. Parmeter, "The challenge of standoff explosives detection," in *Proc. Int. Carnahan Conf. Security Technol.*, Oct. 2004, pp. 355–358.

[6] A. N. Garroway, M. L. Buess, J. B. Miller, B. H. Suits, A. D. Hibbs, G. A. Barrall, *et al.*, "Remote sensing by nuclear quadrupole resonance," *IEEE Trans. Geosci. Remote Sens.*, vol. 39, no. 6, pp. 1108–1118, Jun. 2001.

[7] J. A. S. Smith, "Nitrogen-14 quadrupole resonance detection of RDX and HMX based explosives," in *Proc. Eur. Convent. Security Detect.*, May 1995, pp. 288–292.

[8] A. D. Hibbs, G. A. Barrall, P. V. Czipott, A. J. Drew, D. M. Gregory, D. K. Lathrop, *et al.*, "Detection of TNT and RDX landmines by stand-off nuclear quadrupole resonance," *Proc. SPIE*, vol. 3710, pp. 454–463, Aug. 1999.

[9] T. N. Rudakov, T. J. Rayner, P. A. Hayes, and K. L. Russeth, "Detection of Explosives by Quadrupole Resonance method: New aspects for security," in *Detection and Disposal of Improvised Explosives* (NATO Security through Science). New York, NY, USA: Springer-Verlag, 2006, pp. 191–204.

[10] G. Ota and H. Itozaki, "Nuclear quadrupole resonance echoes from hexamethylenetetramine," *Solid State Nucl. Magn. Resonance*, vol. 30, nos. 3–4, pp. 135–140, 2006.
[11] T. N. Rudakov, V. T. Mikhaltsevitch, and J. H. Flexman, "Spin-echoes in nitrogen-14 quadrupolar spin-system with axially symmetric electric field gradient tensor," *Solid State Nucl. Magn. Resonance*, vol. 25, nos. 1–3, pp. 112–118, 2004.
[12] Y. Tan, S. L. Tantum, and L. M. Collins, "Kalman filtering for enhanced landmine detection using quadrupole resonance," *IEEE Trans. Geosci. Remote Sens.*, vol. 43, no. 7, pp. 1507–1516, Jul. 2005.
[13] S. D. Somasundaram, A. Jakobsson, and N. R. Butt, "Countering radio frequency interference in single-sensor quadrupole resonance," *IEEE Geosci. Remote Sens. Lett.*, vol. 6, no. 1, pp. 62–66, Jan. 2009.
[14] M. D. Rowe and J. A. S. Smith, "Mine detection by nuclear quadrupole resonance," in *Proc. EUREL Int. Conf. Detect. Abandoned Land Mines, A Humanitarian Imperat. Seeking Tech. Solut.*, Oct. 1996, pp. 62–66.
[15] X. Li and X. Zhang, "Investigation of concealed explosive detection by 14^N-NQR," in *Proc. IAEA Tech. Meeting Combined Devices Humanitarian Demining Explosives Detect.*, 2006, pp. 1–3.
[16] J. A. S. Smith and N. F. Peirson, "Method of and apparatus for nuclear quadrupole resonance testing a sample," U.S. Patent 6 566 873, May 20, 2003.
[17] J. D. Roberts, *ABCs of FT-NMR*. Mill Valley, CA, USA: University Science, 2000.
[18] N. Sun, Y. Liu, H. Lee, R. Weissleder, and D. Ham, "CMOS RF biosensor utilizing nuclear magnetic resonance," *IEEE J. Solid-State Circuits*, vol. 44, no. 5, pp. 1629–1643, May 2009.
[19] N. Sun, T.-J. Yoon, H. Lee, W. Andress, R. Weissleder, and D. Ham, "Palm NMR and 1-chip NMR," *IEEE J. Solid-State Circuits*, vol. 46, no. 1, pp. 342–352, Jan. 2011.
[20] I. Bahl, *Fundamentals of RF and Microwave Transistor Amplifiers*. New York, NY, USA: Wiley, 2009.
[21] X. Zhang, N. Schemm, and S. Balkır, "A novel power amplification scheme for nuclear magnetic resonance/nuclear quadrupole resonance systems," *Rev. Sci. Instrum.*, vol. 82, no. 3, pp. 034707-1–034707-6, 2011.
[22] L. Maloratsky, *Passive Rf & Microwave Integrated Circuits*. Amsterdam, The Netherlands: Elsevier, 2004.
[23] R. J. Baker, *CMOS Circuit Design, Layout, and Simulation*. New York, NY, USA: Wiley, 2011.
[24] N. Schemm, S. Balkir, and M. W. Hoffman, "A 4-μW CMOS front end for particle detection applications," *IEEE Trans. Circuits Syst. II, Exp. Briefs*, vol. 57, no. 2, pp. 100–104, Feb. 2010.
[25] Texas Instruments, Inc. (2009). *TMS320C6748 Fixed/Floating-Point DSP*, Dallas, TX, USA [Online]. Available: http://www.ti.com/lit/ds/symlink/tms320c6748.pdf
[26] Texas Instruments, Inc. (2010). *C6748/46/42 Power Consumption Summary*, Dallas, TX, USA [Online]. Available: http://processors.wiki.ti.com/index.php/C6748/46/42_Power_Consumption_Summary

Xinwang Zhang received the B.S. and M.S. degrees in electronics science and technology from Xi'an Jiaotong University in 2001 and 2005, respectively. He is currently pursuing the Ph.D. degree at the Department of Electrical Engineering, University of Nebraska-Lincoln. His research interests include integration of explosive detection systems, RF transceivers, switching power amplifiers and low noise amplifiers. Other research interests include data converters and audio codecs.

Nathan Schemm received the B.S. and Ph.D. degrees in electrical engineering from the University of Nebraska-Lincoln in 2006 and 2010, respectively. In 2010, he joined Texas Instruments Inc. where he currently works as a Senior Circuit Design Engineer. His research interests include VLSI integration of wireless sensor networks, data converters, and radiation detection applications. Other research interests include CMOS imagers, cellular neural networks, and ultra-wideband technology.

Sina Balkır received the B.S. degree in electrical engineering from Boğaziçi University, Istanbul, Turkey, in 1987, and the M.S and Ph.D. degrees in electrical engineering from Northwestern University, Evanston, IL, USA, in 1989 and 1992, respectively. Between 1992 and 1998, he was with the Department of Electrical and Electronics Engineering, Boğaziçi University working as an Assistant and Associate Professor. He is currently with the Department of Electrical Engineering, University of Nebraska-Lincoln, where he serves as a Professor. His research interests include CAD of VLSI systems, analog VLSI design automation, and focal plane computation arrays for image processing.

Michael W. Hoffman received the B.S. degree from Rice University, Houston, TX, USA, the M.S. degree from the University of Southern California, Los Angeles, and the Ph.D. degree from the University of Minnesota, Twin Cities, all in electrical engineering. From 1985 to 1988, he was a Signal Processing System Engineer in the Space Communications Division, TRW Inc. In 1993, he joined the University of Nebraska-Lincoln, where he currently serves as a Professor. His research interests include data compression, joint source channel coding, and sensor array processing.